Available online at www.sciencedirect.com
ScienceDirect
Journal of Solid State Chemistry 180 (2007) 1957–1966
JOURNAL OF SOLID STATE CHEMISTRY
www.elsevier.com/locate/jssc

Layered ruthenium hexagonal perovskites: The new series $[Ba_2Br_{2-2x}(CO_3)_x][Ba_{n+1}Ru_nO_{3n+3}]$ with $n = 2, 3, 4, 5$

Matthieu Kauffmann, Pascal Roussel*, Francis Abraham

UCCS, Equipe Chimie du Solide, CNRS UMR 8181, ENSC Lille—UST Lille, BP 90108, 59652 Villeneuve d'Ascq cedex, France

Received 6 March 2007; received in revised form 7 May 2007; accepted 22 May 2007
Available online 29 May 2007

Abstract

Single crystals of the title compounds were prepared by solid state reactions from barium carbonate and ruthenium metal using a $BaBr_2$ flux and investigated by X-ray diffraction method using Mo(Kα) radiation and a Charge Coupled Device (CCD) detector. A structural model for the term $n = 2$, $Ba_5Ru_2Br_2O_9$ (**1**) was established in the hexagonal symmetry, space group $P6_3/mmc$, $a = 5.8344(2)$ Å, $c = 25.637(2)$ Å, $Z = 2$. Combined refinement and maximum-entropy method (MEM) unambiguously show the presence of CO_3^{2-} ions in the three other compounds (**2**, **3**, **4**). Their crystal structures were solved and refined in the trigonal symmetry, space group $P\bar{3}ml$, $a = 5.8381(1)$ Å, $c = 15.3083(6)$ Å for the term $n = 3$, $Ba_6Ru_3Br_{1.54}(CO_3)_{0.23}O_{12}$ (**2**), and space group $R\bar{3}m$, $a = 5.7992(1)$ Å, $c = 52.866(2)$ Å and $a = 5.7900(1)$ Å, $c = 59.819(2)$ Å for the terms $n = 4$, $Ba_7Ru_4Br_{1.46}(CO_3)_{0.27}O_{15}$ (**3**), and $n = 5$, $Ba_8Ru_5Br_{1.64}(CO_3)_{0.18}O_{18}$ (**4**), respectively. The structures are formed by the periodic stacking along [0 0 1] of $(n+1)$ hexagonal close-packed $[BaO_3]$ layers separated by a double layer of composition $[Ba_2Br_{2-2x}(CO_3)_x]$. The ruthenium atoms occupy the n octahedral interstices created in the hexagonal perovskite slabs and constitute isolated dimers Ru_2O_9 of face-shared octahedra (FSO) in **1** and isolated trimers Ru_3O_{12} of FSO in **2**. In **3** and **4**, the Ru_2O_9 units are connected by corners either directly (**3**) or through a slab of isolated RuO_6 octahedra (**4**) to form a bidimensional arrangement of RuO_6 octahedra. These four oxybromocarbonates belong to the family of compounds formulated $[Ba_2Br_{2-2x}(CO_3)_x][Ba_{n+1}Ru_nO_{3n+3}]$ where n represents the thickness of the octahedral string in hexagonal perovskite slabs. These compounds are compared to the oxychloride series.

Keywords: Hexagonal perovskite; Ruthenium oxybromides; Ruthenium mixed valence; Layered oxycarbonates

1. Introduction

In the cubic and hexagonal barium-containing perovskite-type oxides, the stacking of compact hexagonal $[BaO_3]$ layers creates octahedral holes occupied by a small metal atom M to give various structures depending on the stacking sequence of the $[BaO_3]$ layers. If a layer (noted c) is surrounded by two different layers, the MO_6 octahedra on both sides of this layer are connected by a corner. On the contrary, if the layer (noted h) is surrounded by two identical layers, the MO_6 octahedra are then face-shared. Except for the simplest hh sequence where 1D-arrangement of face-shared octahedra (FSO) is formed, all the structures are built from a 3D-framework of edge- and corner-shared octahedra. For a given M atom, several sequences can be observed corresponding to various polymorphs with transitions in function of the temperature or the pressure. The example of $BaRuO_3$ is very informative [1]. At atmospheric pressure, $BaRuO_3$ adopts a 9R structure with $(hhc)_3$ stacking sequence and contains Ru_3O_{12} trimers of FSO linked together by corner sharing. At 15 kbar, $BaRuO_3$ transforms to a 4H structure with $(hc)_2$ stacking sequence and Ru_2O_9 dimers of FSO linked together by corner sharing. At 30 kbar, this structure transforms to a 6H structure with $(hcc)_2$ stacking sequence and contains Ru_2O_9 dimers of FSO linked by corner sharing with a layer of isolated octahedra. Finally, a cubic $3c$ perovskite structure is expected for $BaRuO_3$ at about 120 kbar [1]. The introduction of $[Ba_2Cl_2]$ double layers within the $[BaO_3]$ stacking breaks the 3D-arrangement and results in the formation of $[Ba_{n+1}M_nO_{3n+3}]^{2-}$ slabs of n octahedra

*Corresponding author. Fax: +33 3 20 43 68 14.
E-mail address: pascal.roussel@ensc-lille.fr (P. Roussel).

0022-4596/$ - see front matter © 2007 Elsevier Inc. All rights reserved.
doi:10.1016/j.jssc.2007.05.018

thickness in the compounds formulated $[Ba_2Cl_2][Ba_{n+1}M_nO_{3n+3}]$ reported for $M = Ru$ and $n = 2$, 3 [2], 4 [3] and for a mixed site $M = 3.33$ Ru -1.67 Ta and $n = 5$ [4]. In these layered 2D structures, the mean oxidation degree (MOD) of the M metal decreases from $+5$ for $n = 2$ to $+4$ for $n = \infty$ which corresponds to infinite thickness of the 2D fragment i.e. to 3D 9R-$BaRuO_3$. Two similar compounds with $[Ba_2Br_2]$ double layers intercalated in the $[BaO_3]$ stacking have been reported for $n = 4$ and 5 in $Ba_7Ru_4Br_2O_{15}$ [5] and $Ba_8Ru_3Ta_2Br_2O_{18}$ [6], respectively. In the present paper we describe the crystal structure of all the terms for the bromide series from $n = 2$ to 5 that contain only Ru as transition metal in octahedral sites. In fact, presence of carbonate ions in the double barium layers leads to the formula $[Ba_2Br_{2-2x}(CO_3)_x][Ba_{n+1}Ru_nO_{3n+3}]$ for this series. The crystal structure of the term $n = 3$ for the chloride series has been revisited and carbonate ions localized in the double barium layers.

2. Experimental

2.1. Synthesis

The starting materials, $BaCO_3$ (Fisher, 99%), Ru (Touzart and Matignon, 99%) and $BaBr_2{,}2H_2O$ (Prolabo, Rectapur, 99%), were used as received. Two compositions of these reactants corresponding to the stoichiometries 3/3/10 and 3/1/10, respectively, were mixed and heated in an alumina crucible from room temperature to 1100 °C in 10 h. After a 48 h maintenance at this temperature the samples were cooled to 500 °C at 15 °C/h and finally to room temperature by cut off the furnace. After dissolving the excess of $BaBr_2$ with hot water, black hexagonal-plate crystals were found in the two experiments. For each synthesis, several single crystals were tested on a single crystal X-ray diffractometer, hexagonal unit cells are always obtained with the same a-parameter ($a \sim 5.8$ Å) and c-parameter depending on the starting synthesis compositions. For the first one, two types of crystals were identified with $c \sim 25.6$ and 15.3 Å corresponding to $Ba_5Ru_2Br_2O_9$ (**1**) and $Ba_6Ru_3Br_2O_{12}$ (**2**), respectively. For the second one, two other types of crystals with $c \sim 52.9$ and 59.8 Å corresponding to $Ba_7Ru_4Br_2O_{15}$ (**3**) and $Ba_8Ru_5Br_2O_{48}$ (**4**), respectively, were obtained. Several crystals from the two preparations were analyzed by energy dispersive spectroscopy using a JEOL JSM-5300 scanning microscope equipped with a PGT digital spectrometer, confirming the presence of Ba, Ru and Br.

2.2. Crystal structure determination

For structure determinations, crystals of the four compounds were selected, mounted on glass fibers and aligned on a Bruker X8 APEX 2 X-ray diffractometer. Intensities were collected at room temperature using MoKα radiation ($\lambda = 0.71073$ Å) selected by a graphite monochromator. Individual frames were measured using a strategy combining ω and φ scans with a rotation of 0.3° and an acquisition time of 20 s per frame. After every data collection, intensities were reduced and corrected for Lorentz, polarization and background effects using the Saint 7.12 software [7]. Once the data processing was performed, the absorption corrections were computed by a semi-empirical method based on redundancy using the SADABS 2006/1 program [8]. Details of the data collection and refinement are given in Table 1.

Compound **1** crystallizes in the hexagonal system and a crystal structure approach was realized in the centro-symmetric $P6_3/mmc$ space group. The three other compounds crystallize in the trigonal system and the crystal structures were solved in the centro-symmetric space groups $P\bar{3}ml$ for 2 and $R\bar{3}m$ for **3** and **4**. The structures were determined by direct methods using SIR97 program [9], which readily established the heavy atom positions (Ba, Ru, Br). Oxygen atoms were localized from difference Fourier maps. The last cycles of refinement included atomic positions, anisotropic displacement parameters for all non-oxygen atoms, and isotropic displacement parameters for oxygen atoms. Full-matrix least squares structure refinements against F were carried out using the JANA 2000 program [10]. In a first step, the crystal structures were refined without carbonate ions and with the Br atoms in the same positions than the Cl atoms in the analogous chlorides which correspond, for $n = 4$ and 5, to the positions used in the previously reported $Ba_7Ru_4Br_2O_{15}$ [5] and $Ba_8Ru_3Ta_2Br_2O_{18}$ [6]. The obtained structural parameters (hereafter the ideal model) are in good agreement with the previously reported results and are given in Table 2 for compound **3**, as example. However, large unusual values of the displacement parameters for Br atoms, particularly in the (0 0 1) plane, were obtained for the four compounds. Furthermore, significant residual electron densities were observed around the bromine sites. This fact strongly suggests that one should apply additional structure refinements, e.g. using displacement parameters together with lowering the site-symmetry for bromine atoms and/or further thermal parameters. For many types of disorder it is difficult to derive an appropriate model based on atoms and harmonic displacement parameters. It can be necessary to use many different sites with a partial occupancy of the atoms. Alternatively, information on disorder can be obtained from a Fourier map generated from the phases of the structure factors calculated for the "best" model and their observed intensities. Another possibility lies in the use of the maximum-entropy method (MEM), a model-free method which may be used for calculating electron densities in solids using experimental phased structure factors as input [11–14]. To calculate the precise electron density (ED) distribution, the MEM analysis was carried out with the computer program BAYMEM [15]. In the present analysis, the total number of electrons in the unit cell was fixed to the $F(0\,0\,0)$ values (1020, 634, 2274 and 2646 e^- for **1**, **2**, **3**, **4**, respectively) and the unit cell was divided into a grid of

Table 1
Crystal data, intensity collection and structure refinement parameters for $Ba_5Ru_2Br_2O_9$ (**1**), $Ba_6Ru_3Br_{1.54}(CO_3)_{0.23}O_{12}$ (**2**), $Ba_7Ru_4Br_{1.46}(CO_3)_{0.27}O_{15}$ (**3**) and $Ba_8Ru_5Br_{1.64}(CO_3)_{0.18}O_{18}$ (**4**)

	1	**2**	**3**	**4**
Crystallographic data				
Formula weight ($g\,mol^{-1}$)	1192.7	1456.2	1738.6	2035.1
Crystal system	Hexagonal	Trigonal	Trigonal	Trigonal
Space group	$P6_3/mmc$	$P\text{-}3m1$	$R\text{-}3m$	$R\text{-}3m$
Unit cell dimensions (Å)	$a = 5.8344(2)$	$a = 5.8381(1)$	$a = 5.7992(1)$	$a = 5.7900(1)$
	$c = 25.637(2)$	$c = 15.3083(6)$	$c = 52.866(2)$	$c = 59.819(2)$
Cell volume ($Å^3$)	755.77(7)	451.86(2)	1539.73(7)	1736.71(7)
Z	2	1	3	3
Density calculated ($g\,cm^{-3}$)	5.24	5.35	5.62	5.88
$F(0\,0\,0)$	1020	625	2241	2625
Crystal size	$120 \times 60 \times 20$	$130 \times 70 \times 20$	$140 \times 90 \times 30$	$150 \times 90 \times 30$
Intensity collection				
Wavelength (Å)	0.71073	0.71073	0.71073	0.71073
2 Theta range (deg)	3.18–84.64	2.66–87.26	4.62–96.50	2.04–82.20
Index range	$-11 \leqslant h \leqslant 9$	$-10 \leqslant h \leqslant 11$	$-7 \leqslant h \leqslant 11$	$-10 \leqslant h \leqslant 10$
	$-9 \leqslant k \leqslant 11$	$-10 \leqslant k \leqslant 11$	$-12 \leqslant k \leqslant 8$	$-10 \leqslant h \leqslant 10$
	$-48 \leqslant l \leqslant 43$	$-23 \leqslant l \leqslant 29$	$-73 \leqslant l \leqslant 106$	$-109 \leqslant h \leqslant 95$
Reflections collected	21 589	14 011	13 472	18 600
Reflections observed	13 719	9608	10 510	11 766
Criterion for observation	$I > 3\sigma(I)$	$I > 3\sigma(I)$	$I > 3\sigma(I)$	$I > 3\sigma(I)$
R_{int} before abs. corr.	0.2696	0.1898	0.1732	0.1667
Absorption correction	SADABS	SADABS	SADABS	SADABS
T_{min}/T_{max}	0.51	0.68	0.62	0.63
R_{int} after abs. corr.	0.0720	0.0607	0.0352	0.0597
Redundancy	19.97	10.12	6.70	12.10
μ (MoKα) (mm^{-1})	20.065	18.731	18.940	19.453
Refinement				
Data/restrains/parameters	1074/0/20	1385/1/42	2010/1/50	1537/1/54
Weighting scheme	Unit	Unit	Unit	Unit
Ideal model				
Final R indices (R, $wR)_{obs}$	0.1221/0.1198	0.0736/0.0809	0.0479/0.0541	0.0554/0.0603
Final R indices (R, $wR)_{all}$	0.1472/0.1309	0.0885/0.1052	0.0604/0.0602	0.0772/0.0900
Max, min $\Delta\rho$ ($e^- Å^3$)	18.99/−19.30	23.23/−6.96	15.05/−8.40	9.47/−11.88
Split-atom model without CO_3				
Final R indices (R, $wR)_{obs}$	–	0.0625/0.0716	0.0373/0.0448	0.0488/0.0538
Final R indices (R, $wR)_{all}$	–	0.0766/0.0979	0.0500/0.0517	0.0703/0.0854
Max, min $\Delta\rho$ ($e^- Å^3$)	–	8.71/−7.77	7.59/−6.14	7.54/−9.81
Split-atom model with CO_3				
Final R indices (R, $wR)_{obs}$	–	0.0540/0.0619	0.0298/0.0354	0.0457/0.0492
Final R indices (R, $wR)_{all}$	–	0.0688/0.0942	0.0423/0.0435	0.0670/0.0841
Final R indices (R, $wR)_{mem}$	–	0.0628/0.0430	0.0260/0.0128	0.0462/0.0326
Max, min $\Delta\rho$ ($e^- Å^3$)	–	6.72/−3.97	5.63/−2.81	7.05/−9.10
Extinction coefficient	0	0	0.070(4)	0

$72 * 72 * 486$ pixels to ensure a good spatial resolution (better than 0.081 Å for all the studied compounds). All independent reflections were used in the process. A particular attention was paid to the strategy of the data collection in order to obtain high angle data (up to $2\theta = 96.5^\circ$ for $Ba_7Ru_4Br_2O_{15}$, for example). All calculations were performed with an initial flat ED. The reliability factor of the MEM, R_{MEM} is indicated in Table 1, with $R_{MEM} = \sum |F_{obs} - F_{MEM}| / \sum |F_{obs}|$, where F_{obs} is obtained by the structural refinement and F_{MEM} is the structure factor calculated from the ED obtained by the MEM.

The visualized three- (3D) and two-dimensional (2D) ED images are shown on Fig. 1a in the region of the bromine atom for **3**, as example. These images clearly showed that the ED at the Br (6*c*) site broadened like a triangular form indicating that bromine ions are distributed over three split sites in a 18*h* site (Br(1)). In the same manner, the Ba(1) site displayed a triangular shape indicating a small splitting over the 3-fold axis. The Ba(2) site showed a slightly elongated ED with an egg-shape (Fig. 1b) indicating a two position splitting. The disorder observed using the MEM was then introduced in the refinement process and therefore the ideal structure model was modified in such a way

Table 2
Atomic coordinates and isotropic displacement parameters for the average structure of 3 corresponding to $Ba_7Ru_4Br_2O_{15}$

Atom	Wyck.	Occ.	x	y	z	U_{iso} or U_{eq}
Ba(1)	6*c*	1	0	0	0.20567(2)	0.0236(2)
Ba(2)	6*c*	1	0	0	0.91766(1)	0.0117(1)
Ba(3)	6*c*	1	0	0	0.28692(1)	0.0085(1)
Ba(4)	3*a*	1	0	0	0	0.0105(2)
Ru(1)	6*c*	1	0	0	0.59518(2)	0.0067(1)
Ru(2)	6*c*	1	0	0	0.64672(1)	0.0054(1)
O(2)	18*h*	1	0.4949(5)	−0.4949(5)	0.08902(9)	0.012(1)
O(3)	18*h*	1	0.8190(5)	−0.8190(5)	0.95596(8)	0.0086(9)
O(4)	9*e*	1	1/2	0	0	0.010(1)
Br(1)	6*c*	1	0	0	0.14228(5)	0.061(1)
Atom	U_{11}	U_{22}	U_{33}	U_{12}	U_{13}	U_{23}
Ba(1)	0.0293(3)	0.0293(3)	0.0121(3)	0.0147(1)	0	0
Ba(2)	0.0092(1)	0.0092(1)	0.0167(3)	0.00462(7)	0	0
Ba(3)	0.0079(1)	0.0079(1)	0.0099(2)	0.00393(6)	0	0
Ba(4)	0.0079(2)	0.0079(2)	0.0157(3)	0.00393(9)	0	0
Ru(1)	0.0056(1)	0.0056(1)	0.0089(3)	0.00278(7)	0	0
Ru(2)	0.0049(1)	0.0049(1)	0.0066(2)	0.00244(7)	0	0
O(2)	0.014(1)	0.014(1)	0.011(1)	0.010(1)	−0.0027(6)	0.0027(6)
O(3)	0.009(1)	0.009(1)	0.009(1)	0.005(1)	0.0005(6)	−0.0005(6)
O(4)	0.011(2)	0.006(2)	0.012(2)	0.003(1)	0.0007(8)	0.001(2)
Br(1)	0.081(2)	0.081(2)	0.0210(9)	0.0408(8)	0	0

Anisotropic displacement parameters.

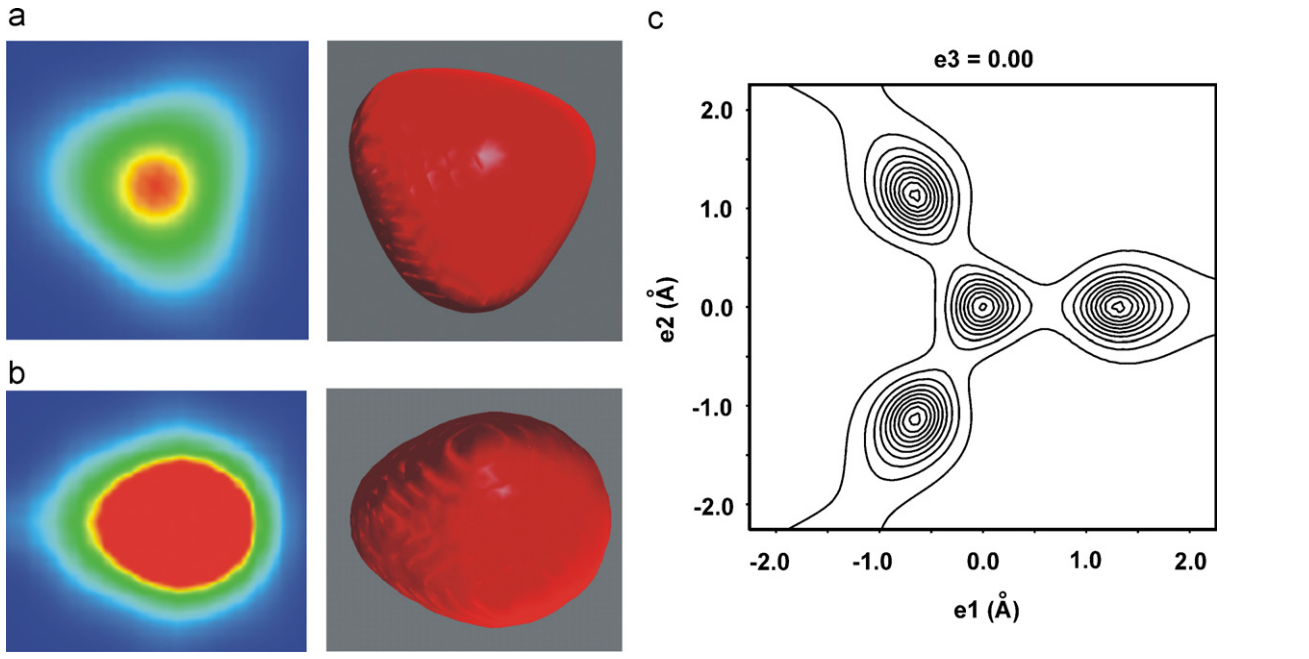

Fig. 1. Electron density representation calculated using the maximum entropy method for compound **3**: (a) 2D and 3D view of Br(1) atom; (b) 2D and 3D view of Ba(2) atom; and (c) 2D contour view of the carbonate ion.

that Br(1) and Ba(1) ions at the 6*c* sites were divided into three positions, corresponding to one third of 18*h* sites, while Ba(2) was split over two 6*c* positions. The occupancy parameters of the Ba ions were constrained to unity to fulfil the chemical composition ($Ba_7Ru_4Br_2O_{15}$ at this stage). This model is called the split-atom model without CO_3 and allows reducing considerably the residual density in all structures (see Table 1). Finally, analysis of the ED also showed a density in form of clover centered on a 6*c* position with three petals corresponding to a 18*h* position with distances compatible with a carbonate ion (Fig. 1c). Therefore a carbonate ion was introduced with an

occupancy factor adjusted to respect the electro-neutrality of the compound considering the same oxidation degree of the ruthenium as in the corresponding oxychloride (see the discussion below). Henceforth this model is called the split-atom model with CO_3. The refinement was somewhat improved ($R_{obs} = 0.0298$ and $wR_{obs} = 0.0354$ to compare to $R_{obs} = 0.0479$ and $wR_{obs} = 0.0541$ for the ideal model) and the residual densities were acceptable (Max $\Delta\rho = 5.63\,e^-/Å^3$ in the split-atom model with CO_3 to compare to $15.05\,e^-/Å^3$). Another formalism which was proved to lead to a good fit to the data is the formalism of anharmonic displacement parameters [16]. This model was tested in the present study but without significant improvements of the R factors and with many parameters and consequently strong correlations. The "simple" split-atom model with CO_3 was then used in the final refinement. All the details and results are given in Table 1. The MEM analysis was conducted in the same way on all the prepared compounds and leads to the same conclusions concerning the disorder for compounds **2** and **4**. Ba(1), Ba(2) and Br(1) atoms are split in the same manner than in $Ba_7Ru_4Br_2O_{15}$ and CO_3 carbonate ions localized. In summary, all the atoms in the vicinity of the $[Ba_2Br_2]$ layers are disordered, whereas the rest of the structure is perfectly ordered. For compound **1**, ED was observed in the vicinity of Br(1) atoms and between the Ba(1) and Ba(2) layers. Unfortunately, in spite of many hypotheses and tests, the results of the structural refinement could not significantly be improved. Thus only the structural approach leading to the average model (Table 3) is considered in this paper for compound **1**. Considering these results, MEM analysis was carried out using the diffraction data collected for the oxychloride compound $Ba_6Ru_3Cl_2O_{12}$ reported in [2] for which high atomic displacement parameter was refined for the chlorine atom. Analogous conclusions were obtained, carbonate ions are unambiguously observed within the double $[Ba_2Cl_2]$ layers and the split-atom model leads to the formula $Ba_6Ru_3Cl_{1.36}(CO_3)_{0.32}O_{12}$ and to an improvement of the refinement ($R_{obs} = 0.0323$ and $wR_{obs} = 0.0321$ to compare to $R_{obs} = 0.0391$ and $wR_{obs} = 0.0572$).

3. Crystal structures descriptions and discussion

The atomic coordinates and displacement parameters are given in Tables 4–6 for **2**–**4**, respectively. Selected bond lengths are listed in Table 7. Valence bond sums were calculated using the expression of bond valence S_{ij} between two atoms i and j given by Brown [17], $S_{ij} = \exp(R_0 - R_{ij})b$ where R_{ij} are the observed bond distances and R_0 and b are empirical constants. For these calculations $R_0 = 1.834$ Å for Ru^{4+} [18] and 1.888 Å for Ru^{5+} [19] with the commonly taken b value, $b = 0.37$ Å [20] were used. The crystal structures of the four compounds $Ba_5Ru_2Br_2O_9$ (**1**), $Ba_6Ru_3Br_{1.54}(CO_3)_{0.23}O_{12}$ (**2**), $Ba_7Ru_4Br_{1.46}(CO_3)_{0.27}O_{15}$ (**3**) and $Ba_8Ru_5Br_{1.64}(CO_3)_{0.18}O_{18}$ (**4**) can be described as an intergrowth of $[Ba_{n+1}Ru_nO_{3n+3}]^{2-}$ anionic hexagonal perovskite slabs and $[Ba_2Br_{2-2x}(CO_3)_x]^{2+}$ double layers and thus can be formulated $[Ba_2Br_{2-2x}(CO_3)_x][Ba_{n+1}Ru_nO_{3n+3}]$ with $n = 2, 3, 4, 5$ for **1**, **2**, **3**, **4**, respectively.

3.1. The stacking sequences

The four structures can be described from the stacking along the c-axis of $[BaO_3]$ and [BaBr] layers in various sequences. In [BaBr] layers, the barium atoms occupy the same positions as in the corresponding $[BaO_3]$ layers but the oxygen atoms are removed. So in the stacking sequence they are noted with a $'$ to indicate the deficient [BaBr] layers. The four compounds differ by the number $(n+1)$ of successive $[BaO_3]$ layers, $n = 2, 3, 4, 5$ for compounds **1**, **2**, **3**, **4**, respectively, resulting in the formation of $[BaO_3]_{n+1}$ slabs stacked in the [0 0 1] direction and separated by two [BaBr] layers. For the two first terms the slabs contain only two types of $[BaO_3]$ layers leading to (*hhh*) and (*hhhh*)

Table 3
Atomic coordinates and isotropic displacement parameters for the average structure of $Ba_5Ru_2Br_2O_9$ (**1**)

Atom	Wyck.	Occ.	x	y	z	U_{iso} or U_{eq}
Ba(1)	4*f*	1	1/3	2/3	0.91916(1)	0.0393(9)
Ba(2)	4*f*	1	1/3	2/3	0.17207(8)	0.0140(4)
Ba(3)	2*d*	1	1/3	2/3	3/4	0.0116(5)
Ru(1)	4*e*	1	0	0	0.19579(9)	0.0096(4)
O(2)	12*k*	1	0.164(2)	0.328(3)	0.8424(5)	0.017(2)
O(3)	6*h*	1	0.146(1)	0.292(3)	1/4	0.002(2)
Br(1)	4*f*	1	1/3	2/3	0.4520(3)	0.094(4)
Atom	U_{11}	U_{22}	U_{33}	U_{12}	U_{13}	U_{23}
Ba(1)	0.049(1)	0.049(1)	0.0189(9)	0.0247(6)	0	0
Ba(2)	0.0117(4)	0.0117(4)	0.0185(7)	0.0059(2)	0	0
Ba(3)	0.0081(5)	0.0081(5)	0.0187(9)	0.0041(3)	0	0
Ru(1)	0.0075(5)	0.0075(5)	0.0138(8)	0.0038(2)	0	0
Br(1)	0.126(6)	0.126(6)	0.028(3)	0.063(3)	0	0

Anisotropic displacement parameters for the non-oxygen atoms.

Table 4
Atomic coordinates and isotropic displacement parameters for $Ba_6Ru_3O_{12}Br_{1.54}(CO_3)_{0.23}$ (**2**)

Atom	Wyck.	Occ.	x	y	z	U_{iso} or U_{eq}
Ba(1)	6*i*	0.333	0.658(4)	−0.658(4)	0.6331(1)	0.022(2)
Ba(2a)	2*d*	0.916(8)	$\frac{1}{3}$	$\frac{2}{3}$	0.7898(1)	0.0108(3)
Ba(2b)	2*d*	0.084(8)	$\frac{1}{3}$	$\frac{2}{3}$	0.760(2)	0.0108(3)
Ba(3)	2*d*	1	$\frac{1}{3}$	$\frac{2}{3}$	0.07789(9)	0.0117(2)
Ru(1)	2*c*	1	0	0	0.8271(1)	0.0090(3)
Ru(2)	1*a*	1	0	0	0	0.0076(3)
Br(1)	6*i*	0.257(6)	0.320(6)	−0.320(6)	0.5838(3)	0.037(5)
C(1)	2*c*	0.115(9)	0	0	0.44(1)	0.0150
O(1)	6*i*	0.115(9)	0.124(9)	−0.124(9)	0.566(5)	0.0150
O(2)	6*i*	1	0.162(1)	−0.162(1)	0.2324(6)	0.014(2)
O(3)	6*i*	1	0.8451(9)	−0.8451(9)	0.0791(5)	0.011(2)
Atom	U_{11}	U_{22}	U_{33}	U_{12}	U_{13}	U_{23}
Ba(1)	0.026(4)	0.026(4)	0.0159(6)	0.014(2)	0.003(2)	−0.003(2)
Ba(2a)	0.0096(3)	0.0096(3)	0.0132(8)	0.0048(1)	0	0
Ba(2b)	0.0096(3)	0.0096(3)	0.0132(8)	0.0048(1)	0	0
Ba(3)	0.0093(3)	0.0093(3)	0.0166(5)	0.0046(1)	0	0
Ru(1)	0.0070(3)	0.0070(3)	0.0130(5)	0.0035(1)	0	0
Ru(2)	0.0058(4)	0.0058(4)	0.0111(7)	0.0029(2)	0	0
Br(1)	0.043(6)	0.043(6)	0.012(2)	0.011(9)	0.005(3)	−0.005(3)
O(2)	0.015(3)	0.015(3)	0.016(3)	0.010(3)	−0.003(1)	0.003(1)
O(3)	0.012(2)	0.012(2)	0.011(3)	0.008(3)	0.001(1)	−0.001(1)

Anisotropic displacement parameters for the non-carbonate atoms.

Table 5
Atomic coordinates and isotropic displacement parameters for $Ba_7Ru_4O_{15}Br_{1.46}(CO_3)_{0.27}$ (**3**)

Atom	Wyck.	Occ.	x	y	z	U_{iso} or U_{eq}
Ba(1)	18*h*	0.333	0.0065(6)	−0.0065(6)	0.20556(2)	0.0231(6)
Ba(2a)	6*c*	0.919(8)	0	0	0.91787(3)	0.0100(2)
Ba(2b)	6*c*	0.081(8)	0	0	0.9112(3)	0.0100(2)
Ba(3)	6*c*	1	0	0	0.28691(1)	0.00872(8)
Ba(4)	3*a*	1	0	0	0	0.0107(1)
Ru(1)	6*c*	1	0	0	0.59517(1)	0.00688(9)
Ru(2)	6*c*	1	0	0	0.64672(1)	0.00568(9)
Br(1)	18*h*	0.243(3)	0.014(2)	−0.014(2)	0.14232(4)	0.039(2)
C(1)	6*c*	0.135(4)	0	0	0.482(1)	0.0150
O(1)	18*h*	0.135(4)	0.125(3)	−0.125(3)	0.5180(5)	0.0150
O(2)	18*h*	1	0.4948(4)	−0.4948(4)	0.08886(7)	0.0125(9)
O(3)	18*h*	1	0.8191(3)	−0.8191(3)	0.95597(6)	0.0085(7)
O(4)	9*e*	1	1/2	0	0	0.010(1)
Atom	U_{11}	U_{22}	U_{33}	U_{12}	U_{13}	U_{23}
Ba(1)	0.0309(8)	0.0309(8)	0.0130(2)	0.0196(9)	−0.0045(4)	0.0045(4)
Ba(2a)	0.0091(1)	0.0091(1)	0.0119(4)	0.00453(5)	0	0
Ba(2b)	0.0091(1)	0.0091(1)	0.0119(4)	0.00453(5)	0	0
Ba(3)	0.00803(9)	0.00803(9)	0.0101(1)	0.00402(5)	0	0
Ba(4)	0.0080(1)	0.0080(1)	0.0160(3)	0.00401(6)	0	0
Ru(1)	0.0058(1)	0.0058(1)	0.0091(2)	0.00289(5)	0	0
Ru(2)	0.0051(1)	0.0051(1)	0.0068(2)	0.00255(5)	0	0
Br(1)	0.041(2)	0.041(2)	0.0116(7)	0.002(4)	0.004(1)	−0.004(1)
O(2)	0.014(1)	0.014(1)	0.012(1)	0.010(1)	−0.0028(5)	0.0028(5)
O(3)	0.0085(7)	0.0085(7)	0.0093(9)	0.0048(8)	0.0004(4)	−0.0004(4)
O(4)	0.011(1)	0.007(1)	0.013(2)	0.0034(7)	0.0008(6)	0.002(1)

Anisotropic displacement parameters for the non-carbonate atoms.

Table 6
Atomic coordinates and isotropic displacement parameters for $Ba_8Ru_5O_{18}Br_{1.66}(CO_3)_{0.17}$ (**4**)

Atom	Wyck.	Occ.	x	y	z	U_{iso} or U_{eq}
Ba(1)	18*h*	0.333	0.011(3)	−0.011(3)	0.36796(4)	0.022(2)
Ba(2a)	6*c*	0.90(4)	0	0	0.7413(2)	0.0114(7)
Ba(2b)	6*c*	0.10(4)	0	0	0.736(1)	0.0114(7)
Ba(3)	6*c*	1	0	0	0.44046(2)	0.0103(2)
Ba(4)	6*c*	1	0	0	0.81193(2)	0.0108(2)
Ru(1)	6*c*	1	0	0	0.08422(3)	0.0086(3)
Ru(2)	6*c*	1	0	0	0.13025(3)	0.0073(3)
Ru(3)	3*b*	1	0	0	$\frac{1}{2}$	0.0165(6)
Br(1)	18*h*	0.277(7)	0.983(3)	−0.983(3)	0.31205(9)	0.062(5)
C(1)	6*c*	0.08(1)	0	0	0.006(5)	0.0150
O(1)	18*h*	0.08(1)	0.87(1)	−0.87(1)	0.016(2)	0.0150
O(2)	18*h*	1	0.161(1)	−0.161(1)	0.0687(1)	0.014(3)
O(3)	18*h*	1	0.1525(9)	−0.1525(9)	0.8916(1)	0.010(2)
O(4)	18*h*	1	0.164(1)	−0.164(1)	0.1476(1)	0.012(2)
Atom	U_{11}	U_{22}	U_{33}	U_{12}	U_{13}	U_{23}
Ba(1)	0.024(2)	0.024(2)	0.0142(6)	0.007(2)	−0.003(1)	0.003(1)
Ba(2a)	0.0114(3)	0.0114(3)	0.011(2)	0.0057(2)	0	0
Ba(2b)	0.0114(3)	0.0114(3)	0.011(2)	0.0057(2)	0	0
Ba(3)	0.0093(3)	0.0093(3)	0.0122(4)	0.0047(1)	0	0
Ba(4)	0.0100(3)	0.0100(3)	0.0122(4)	0.0050(1)	0	0
Ru(1)	0.0080(3)	0.0080(3)	0.0097(5)	0.0040(2)	0	0
Ru(2)	0.0068(3)	0.0068(3)	0.0081(5)	0.0034(2)	0	0
Ru(3)	0.0160(7)	0.0160(7)	0.017(1)	0.0080(3)	0	0
Br(1)	0.056(4)	0.056(4)	0.016(2)	−0.014(9)	−0.009(3)	0.009(3)
O(2)	0.016(3)	0.016(3)	0.014(3)	0.010(3)	0.002(1)	−0.002(1)
O(3)	0.012(2)	0.012(2)	0.010(3)	0.008(3)	−0.001(1)	0.001(1)
O(4)	0.014(3)	0.014(3)	0.009(3)	0.008(3)	−0.002(1)	0.002(1)

Anisotropic displacement parameters for the non-carbonate atoms.

Table 7
Ruthenium–oxygen and ruthenium–ruthenium distances (Å) in $Ba_5Ru_2Br_2O_9$ (**1**), $Ba_6Ru_3Br_{1.54}(CO_3)_{0.23}O_{12}$ (**2**), $Ba_7Ru_4Br_{1.46}(CO_3)_{0.27}O_{15}$ (**3**) and $Ba_8Ru_5Br_{1.64}(CO_3)_{0.18}O_{18}$ (**4**)

	1	**2**	**3**	**4**
	d (Å)	d (Å)	d (Å)	d (Å)
Ru(1)–O(2)	1.92(1) × 3	1.870(7) × 3	1.864(3) × 3	1.862(9) × 3
Ru(1)–O(3)	2.02(1) × 3	2.125(7) × 3	2.110(3) × 3	2.105(6) × 3
Ru(2)–O(3)	–	1.980(7) × 6	1.991(3) × 3	2.012(6) × 3
Ru(2)–O(3)	–	–	1.9785(3) × 3	1.945(7) × 3
Ru(3)–O(3)	–	–	–	2.046(7) × 6
Ru(1)–Ru(2)	2.780(3)	2.647(1)	2.7252(7)	2.753(3)

sequences. For the two other terms, one or two cubic close-packed *c* layers are introduced at the middle of the (*hhhh*) sequence to give (*hhchh*) and (*hhcchh*) sequences. In the four compounds the [BaBr] layers correspond to a ($h'h'$) slab, so the complete layers sequences of both [BaO_3] and [BaBr] layers are $(hhhh'h')_2$ for $n = 2$, $(hhhhh'h')$ for $n = 3$, leading to hexagonal lattices (10H and 6H sequences, respectively) and $(hhchhh'h')_3$ for $n = 4$ and $(hhcchhh'h')_3$ for $n = 5$ with rhombohedral lattice (21R and 24R sequences, respectively).

3.2. The RuO_6 octahedral arrangement

The ruthenium atoms occupy the n octahedral holes created by the [BaO_3] layers leading to $[Ba_{n+1}Ru_nO_{3n+1}]$ slabs. For $n = 2$, 4 and 5, Ru_2O_9 dimers of FSO are formed, they are isolated for $n = 2$, connected by corner sharing for $n = 4$ and through isolated RuO_6 octahedra for $n = 5$. Finally, for $n = 3$, isolated Ru_3O_{12} columns of three FSO are formed. The four slabs can be deduced from the three polytypes of $BaRuO_3$ by separating the blocks on both sides from a shear plane which is a *c* layer (Fig. 2) and, of course, by adding a [BaO_3] layer to border one of the two blocks giving a sheet $[Ba_{n+1}Ru_nO_{3n+1}]$. For $n = 2$ and 4, the slabs are deduced from the same 4H polytype but with a single and a double stage separation respectively. For $n = 3$, the slabs are deduced from the 9R polytype. Finally, the $n = 5$ slabs are obtained from the 6H polytype by withdrawing one layer of isolated RuO_6 octahedra out of two. The $n = 1$ slab could result from the supposed 3C polytype but is unexpected because it would be made only of isolated octahedra. The insertion between the perovskite-type blocks of cationic $[Ba_2Br_{2-2x}(CO_3)_x]^{2+}$ layers leads to 2+ charge of the perovskite-type blocks that implies an oxidation of the ruthenium atom to

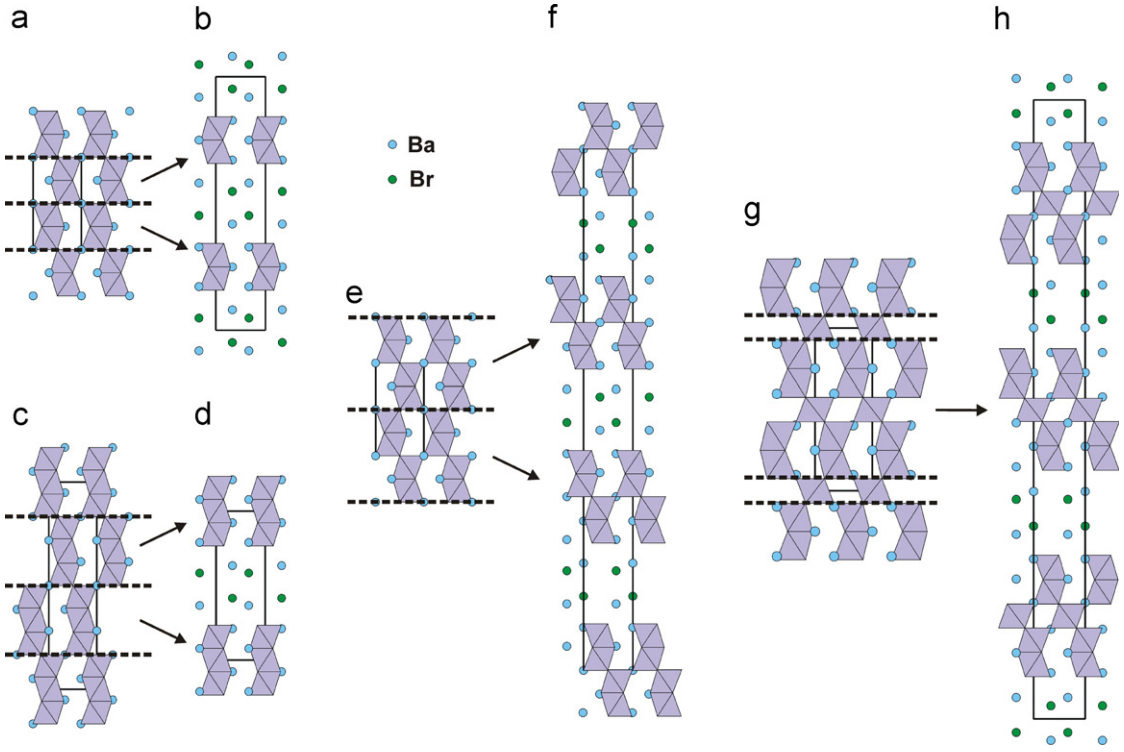

Fig. 2. Projection along [0 1 0] of: (a) 4H-$BaRuO_3$; (b) $Ba_5Ru_2Br_2O_9$ $n=2$; (c) 9R-$BaRuO_3$; (d) $Ba_6Ru_3Br_2O_{12}$ $n=3$; (e) 4H-$BaRuO_3$; (f) $Ba_7Ru_4Br_2O_{15}$ $n=4$; (g) 6H-$BaRuO_3$; and (h) $Ba_8Ru_5Br_2O_{18}$ $n=5$. The four ideal structures of the series $[Ba_2Br_2][Ba_{n+1}Ru_nO_{3n+3}]$ can be deduced from the three polytypes of $BaRuO_3$ by separating the blocks on both sides from a shear plane which is a c layer and by intercalation of $[Ba_2Br_2]$ double layers.

the mean degree $(4+2/n)$. Thus the transformation from $BaRuO_3$ to the oxyhalides compounds can be called oxidative intercalation. The same type of oxidative intercalation of $[Ba_2X_2]$ layers has been recently reported to explain the transformation of $Ba_2Co_9O_{14}$ [21,22] in the oxyhalides $[Ba_2X_2]Ba_2Co_8O_{14}$, $X=Cl$, Br [23].

Dimers of FSO are very common in ruthenium compounds. If the ruthenium atoms were at the center of the neighboring FSO, the Ru–Ru distance, which corresponds to the average thickness of close-packed layers, should be 2.37 Å. The repulsion between Ru atoms which would lead to the destabilization of the structure can be prevented by the formation of a Ru–Ru metal bond as observed in Ru_2O_9 dimers containing Ru^{4+} or Ru at the MOD of +4.5 with Ru–Ru distances smaller than in the metal itself (2.65 Å). For example the Ru–Ru distance is 2.537 Å in 4H-$BaRuO_3$ [24], 2.481–2.515 Å in 6H-$Ba_3M^{4+}Ru_2O_9$, $M=$ Ce, Pr, Tb [25] and Ti [26], and 2.517–2.563 Å in $Ba_3M^{3+}Ru_2O_9$ compounds, $M=$ Y [27,28], in [27,29], La, Nd, Sm–Tb, Ho, Er, Yb, Lu [27,28,30,31]. The Ru^{5+} atom with low spin configuration d^3 is more favorable than the Ru^{4+} atom with low spin configuration d^4 to the formation of Ru–Ru bond. However, in the $Ba_3M^{2+}Ru_2O_9$ compounds, $M=$ Co, Zn [29,32], Mg, Ca, Sr, Cd [33–35], the Ru–Ru distances are in the range from 2.652 to 2.701 Å that indicates that the Ru–Ru metal bond no longer exists. In $Ba_5Ru_2O_9Br_2$, the Ru–Ru distance is even longer (2.780(3) Å) and comparable to that observed in the corresponding oxychloride compound (2.819(4) Å). The Ru^{5+}–Ru^{5+} repulsion is reduced by the shortening of the O(2)–O(2) edge of the common face to 2.56(2) Å. The $[Ba_2X_2][Ba_3Ru_2O_9]$ oxyhalides can be deduced from the $Ba_3M^{2+}Ru_2O_9$ oxides by the replacement of M^{2+} cations by $[Ba_2X_2]^{2+}$ layers between $[Ba_3Ru_2O_9]^{2-}$ slabs that leads to a greater distance between the slabs allowing a lengthening of the intradimer Ru–Ru distance. Finally, the change of the nature of the cationic species between the $[Ba_3Ru_2O_9]$ slabs, monovalent-, divalent-, trivalent-ions or $[Ba_2X_2]^{2+}$ or $[Ba_2(O_2)]^{2+}$ layers [36,37], provides access to the Ru–Ru distances which cover all the range between the Ru–Ru distances reported in Ru_2O_{10} dimers of edge-shared octahedra with strong metal–metal bonding in $La_4Ru_6O_{19}$ (2.488 Å) [38] and no metal–metal bonding in $La_3Ru_3O_{11}$ (2.990 Å) [39].

In **3** and **4** that contain ruthenium at the MOD +4.5 and +4.4, respectively, the Ru–Ru distances within the dimers indicate clearly that there is no metal–metal bond. Furthermore the distances are slightly lower to that calculated in **1**, in agreement with the lower MOD of ruthenium and consequently weaker repulsion. In addition, whereas the average Ru–O distances do not allow to propose a charge distribution on the ruthenium atoms, the bond valence sums (BVS) indicate a tendency showing that ruthenium ions are mainly Ru^{4+} at the Ru(2) site and Ru^{5+} at the Ru(1) site in **3**. On the contrary, in **4**, the greater Ru(3)–O bonds and the smaller BVS value reveals

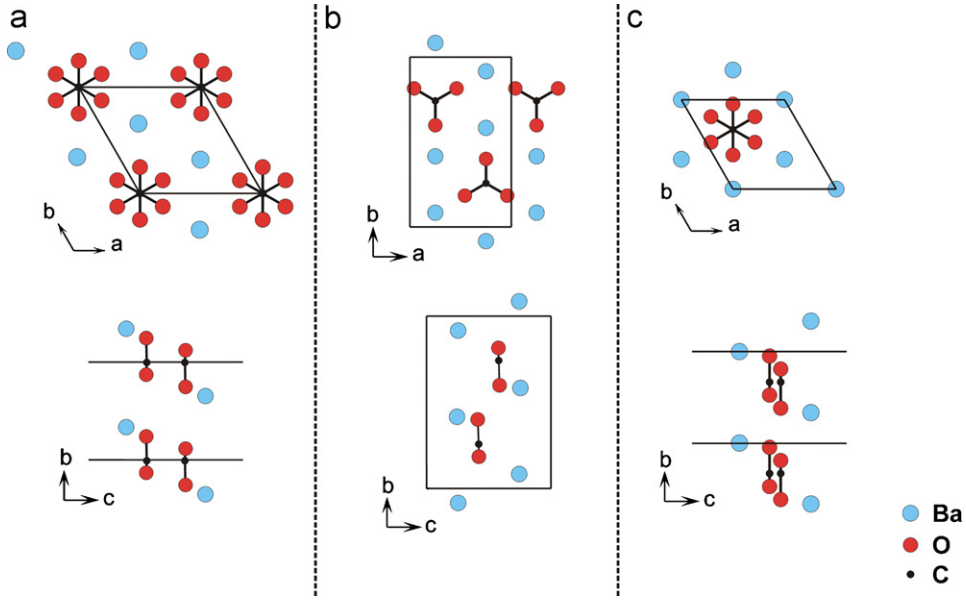

Fig. 3. View along [0 0 1] and [1 0 0] of the $[Ba_2CO_3]$ sheets in: (a) $Ba_6Ru_3Br_{1.54}(CO_3)_{0.23}O_{12}$ with disorder of CO_3 groups; (b) witherite-$BaCO_3$ with aragonite-type structure, and (c) $BaCO_3$-II.

the presence of Ru^{4+} in the $Ru(3)O_6$ octahedra connecting the dimers, thus the charge repartition within the dimers is rather similar in **3** and **4**.

Finally in **2**, the Ru–Ru distance within the trimer FSO is similar to that calculated for the corresponding chlorine compound and greater than in 9R-$BaRuO_3$ [2], in agreement with the increase of MOD. Both the average Ru–O distances and the BVS do not permit to determine unambiguously the charge repartition in the three sites although the most probable distribution is Ru^{5+}–Ru^{4+}–Ru^{5+} as in $Ba_5Ru_3O_{12}$ [19].

3.3. The Br, CO_3 disorder in the $[Ba_2X_2]^{2+}$ layers

In the ideal structure, the Br atoms occupy all the tetrahedral sites created between two [Ba] layers leading to a fluorite type sheet. However, the Ba(2) atoms that border the perovskite slab belong to the coordination polyhedra of the Br atom better described as a trigonal bipyramid. In the actual structure, the C atom of a carbonate anion is located above or below the octahedral site between the [Ba] layers, the oxygen atoms being directed towards the Br atoms that should be removed. So, three Br atoms are replaced by one carbonate anion leading to a slightly lower MOD of the ruthenium atoms or to the formation of clusters of carbonate ions. In fact, one can also suppose the existence of $[Ba_2Br_2]$ layers and $[Ba_2CO_3]$ layers (Fig. 3a) identical to those met in $BaCO_3$. In the mineral witherite [40], with aragonite-type structure, the carbonate anions are displaced from the octahedral site to a tetrahedral one within a hexagonal close-packing of [Ba] layers (Fig. 3b). In $BaCO_3$-II [41], the carbonate ions are disordered on both sides of the octahedral sites (Fig. 3c) as in the currently described compounds. The presence of carbonate ions has been reported in many compounds with perovskite-related structures as, for examples, in high-T_c superconductors [42–45], in Ruddlesden–Popper materials such as $Sr_4Fe_{2-x}M_xO_6CO_3$ (M = Sc, Ni, Co) [46] where they substitute layers of metal octahedra. In 6H-$Ba_3(Ru_{1.69}C_{0.31})(Na_{0.95}Ru_{0.05})O_{8.69}$ [47], part of the Ru_2O_9 dimeric units of the parent compound $Ba_3Ru_2NaO_9$ [48], are replaced by one RuO_5 and one CO_3 group. Finally in $Ba_3Co_2O_6(CO_3)_{0.60}$, carbonate ions and Ba atoms form $[Ba(CO_3)_{0.60}]$ rods, related to the $BaCO_3$ aragonite-type structure, intergrowth with 2H-$[Ba_2Co_2O_6]$ columns [49].

4. Conclusion

Single crystals of the terms $n = 2$, 3, 4 and 5 of the series $[Ba_2Br_{2-2x}(CO_3)_x][Ba_{n+1}Ru_nO_{3n+3}]$ have been isolated. For $n = 2$ and 3, the $[Ba_{n+1}Ru_nO_{3n+3}]^{2-}$ slabs contain, respectively, Ru_2O_9 and Ru_3O_{12} entities resulting from face-shared octahedra (FSO), and giving one-dimensional (1D) ruthenium octahedra arrangement. For $n = 4$ and 5, the $[Ba_{n+1}Ru_nO_{3n+3}]^{2-}$ slabs contain also Ru_2O_9 dimers of face-shared octahedral further connected directly or by layers of isolated RuO_6 octahedra giving 2D arrangements. The mean oxidation state of Ru decreases from +5 for $n = 2$ to +4.4 for $n = 5$. One interesting point of this series is to show the possibility of $[Ba_2CO_3]$ layers between perovskite-type blocks that opens a new way of synthesis of interesting oxycarbonates.

References

[1] J.M. Longo, J.A. Kafalas, Mater. Res. Bull. 3 (1968) 687.
[2] N. Tancret, P. Roussel, F. Abraham, J. Solid State Chem. 177 (2004) 806.

[3] M. Neubacher, Hk. Müller-Buschbaum, Z. Anorg. Allg. Chem. 602 (1991) 143.
[4] J. Wilkens, Hk. Müller-Buschbaum, J. Alloys Compds. 179 (1992) 187.
[5] St. Scheske, Hk. Müller-Buschbaum, J. Alloys Compds. 198 (1993) L25.
[6] J. Wilkens, Hk. Müller-Buschbaum, J. Alloys Compds. 182 (1992) 265.
[7] Bruker Analytical X-ray system, "SAINT+, Version 7.12", Madison, USA, 2004.
[8] G.M. Scheldrick, SADABS, Bruker-Siemens Area Detector Absorption and Other Correction, Version 2006/1, Goetingen, Germany, 2006.
[9] A. Altomare, M.C. Burla, M. Camalli, G. Cascarano, C. Giacovazzo, A. Guagliardi, A.G.G. Moliterni, G. Polidori, R. Spagna, SIR97 A Package for Crystal Structure Solution by Direct Methods and Refinement, Bari, Rome, Italy, 1997.
[10] V. Petricek, M. Dusek L. Palatinus, The Crystallographic Computing System JANA2000, Praha, Czech Republic, 2005.
[11] C.J. Gilmore, Acta Crystallogr. A 52 (1996) 561.
[12] R.J. Papoular, Acta Crystallogr. A 47 (1991) 293.
[13] B. Bagautdinov, J. Luedecke, M. Schneider, S. van Smaalen, Acta Cryst. B 54 (1998) 626.
[14] M. Sakata, M. Sato, Acta Crystallogr. A 46 (1990) 263.
[15] L. Palatinus, S. Van Smaalen, BAYMEM—a computer program for application of the maximum entropy method in reconstruction of electron densities in arbitrary dimension, 2005.
[16] W.F. Kuhs, Acta Crystallogr. A 48 (1992) 80.
[17] I.D. Brown, in: M. O'Keefe, A. Navrotsky (Eds.), Structure and Bonding in Crystals, vol. II, Academic Press, New York, 1980, pp. 1–30.
[18] M.E. Brese, M. O'Keefe, Acta Crystallogr. B 47 (1991) 192.
[19] C. Dussarat, F. Grasset, R. Bontchev, J. Darriet, J. Alloys Compds. 233 (1996) 15.
[20] Brown, Altermatt, Acta Crystallogr. B 41 (1985) 244.
[21] J. Sun, M. Yang, G. Li, T. Yang, F. Liao, Y. Wang, M. Xiong, J. Lin, Inorg. Chem. 45 (2006) 9151.
[22] G. Ehora, S. Daviero-Minaud, M. Colmont, G. André, O. Mentré, Chem. Mater. 19 (2007) 2180.
[23] M. Kauffmann, N. Tancret, F. Abraham, P. Roussel, Solid State Science (2007), accepted for publication.
[24] S.-T. Hong, A.W. Sleight, J. Solid State Chem. 132 (1997) 407.
[25] Y. Doi, M. Wakeshima, Y. Hinatsu, A. Tobo, K. Ohoyama, Y. Yamagushi, J. Mater. Chem. 11 (2001) 3135.
[26] D. Verdoes, H.W. Zandbergen, D.J.W. Ijdo, Acta Crystallogr. C 41 (1985) 170.
[27] Y. Doi, K. Matsuhira, Y. Hinatsu, J. Solid State Chem. 165 (2002) 317.
[28] M. Rath, Hk. Müller-Buschbaum, J. Alloys Compds. 210 (1994) 119.
[29] J.T. Rijssenbeek, Q. Huang, R.W. Erwin, H.W. Zandbergen, R.J. Cava, J. Solid State Chem. 146 (1999) 65.
[30] Y. Doi, Y. Hinatsu, J. Mater. Chem. 12 (2002) 1792.
[31] Y. Doi, Y. Hinatsu, Y. Shimojo, Y. Ishii, J. Solid State Chem. 161 (2001) 113.
[32] P. Lightfoot, P.D. Battle, J. Solid State Chem. 89 (1990) 174.
[33] J. Darriet, M. Drillon, G. Villeneuve, P. Hagenmuller, J. Solid State Chem. 19 (1976) 213.
[34] J. Darriet, J.L. Soubeyroux, A.P. Murani, J. Phys. Chem. Solids 44 (3) (1983) 269.
[35] H.W. Zandbergen, D.J.W. Ijdo, Acta Crystallogr. C 40 (1984) 919.
[36] F. Grasset, M. Zakhour, J. Darriet, J. Alloys Compds. 287 (1999) 25.
[37] F. Grasset, C. Dussarat, J. Darriet, J. Mater. Chem. 7 (9) (1997) 1911.
[38] F. Abraham, J. Trehoux, D. Thomas, Mater. Res. Bull. 12 (1977) 43.
[39] F. Abraham, J. Trehoux, D. Thomas, Mater. Res. Bull. 13 (1978) 805;
A. Cotton, C.E. Rice, J. Solid State Chem. 25 (1978) 137.
[40] C.M. Holl, J.R. Smith, H.M.S. Laustsen, S.D. Jacobsen, R.T. Downs, Phys. Chem. Miner. 27 (2000) 467.
[41] K.O. Stromm, Acta Chem. Scand. Ser A 29 (1975) 105.
[42] M. Huvé, C. Michel, A. Maignan, M. Hervieu, C. Martin, B. Raveau, Physica C 205 (1993) 219.
[43] C. Greaves, R.P. Slater, Physica C 175 (1991) 172.
[44] B. Domengès, M. Hervieu, B. Raveau, Physica C 207 (1993) 65.
[45] M. Hervieu, P. Boullay, B. Domengès, A. Maignan, B. Raveau, J. Solid State Chem. 105 (1993) 300.
[46] Y. Bréard, C. Michel, A. Maignan, F. Studer, B. Raveau, Chem. Mater. 15 (2003) 1273.
[47] E. Quarez, M. Huvé, F. Abraham, O. Mentré, Solid State Sci. 5 (2003) 951.
[48] K.E. Stitzer, M.D. Smith, W.R. Gemmill, H.-C. zur Loye, J. Am. Chem. Soc. 124 (2002) 13877.
[49] K. Boulahya, U. Amador, M. Parras, J.M. Gonzales-Calbert, Chem. Mater. 12 (2000) 966.